Reaction Kinetics, Mechanisms and Catalysis
https://doi.org/10.1007/s11144-024-02663-5

Cobalt-doped graphitic carbon nitride for hydrogen production under visible light

Khursheed Ahmad[1] · Waseem Raza[2] · Ali Alsulmi[3] · Mohd Quasim Khan[4]

Received: 3 April 2024 / Accepted: 20 May 2024

Abstract

Herein, we reported the synthesis of cobalt (Co)-doped graphitic carbon nitride (Co@g-C_3N_4) and its application in photocatalytic H_2 production. The formation, phase, crystalline nature, surface morphology, and elemental composition of the Co@g-C_3N_4 have been examined by XRD, SEM, XPS, and EDX spectroscopy. The platinum has been introduced as a cocatalyst and Co@g-C_3N_4/Pt (3 wt%) exhibited excellent photocatalytic performance towards the generation of H_2. The synthesized Co@g-C_3N_4/Pt (3 wt%) material exhibited a significant amount of H_2 production rate of 6347 μmol/g surpassing that of Co@g-C_3N_4 in the presence of TEOA sacrificial agent. The improved photocatalytic performance of the synthesized photocatalyst can be attributed to the synergistic interaction and Schottky barrier formation among Pt, Co, and g-C_3N_4, facilitating efficient charge separation and transportation of photo-induced charge carriers. This study has the potential to open up new avenues for addressing energy and environmental challenges through H_2 production.

Keywords Co@g-C_3N_4 · Graphitic-carbon nitride · Hydrogen production · Photocatalysis

✉ Mohd Quasim Khan
quasimkhanmohd90@gmail.com

[1] School of Materials Science and Engineering, Yeungnam University, Gyeongsan 38541, Republic of Korea

[2] Regional Center of Advanced Technologies and Materials, Šlechtitelů 27, 78371 Olomouc, Czech Republic

[3] Department of Chemistry, College of Science, King Saud University, Riyadh 11451, Kingdom of Saudi Arabia

[4] Department of Chemistry, M.M.D.C, Moradabad, M.J.P. Rohilkhand University, Bareilly 244001, U.P, India

Published online: 23 May 2024

Introduction

Recently, it has been reported that energy demand will be significantly enhanced in the next decades which may cause an energy crisis [1–3]. The increasing global population and its consequent economic activities have created a relentless demand for energy [4–7]. In the present scenario, fossil fuels contribute 84% of the world's energy supply [8–15] However, the swift depletion of fossil fuel reserves, coupled with environmental pollution and the looming threat of global warming, underscores the pressing need to explore alternative, eco-friendly, and renewable energy sources [16–19] In recent years, significant strides have been made in utilizing solar energy for water splitting, a process that converts water into hydrogen and oxygen, thus offering a promising renewable energy solution [20, 21]. Hydrogen gas (H_2) emerges as a top contender for future solar energy fuels [22, 23], boasting the highest energy density (~ 120 MJ/kg) among all known fuels and being readily available on Earth in various forms such as water, organic matter, and hydrocarbons [24, 25]. Several methods exist for generating H_2, including natural gas steam reforming, partial methanol oxidation, coal gasification, thermochemical water splitting, high-temperature electrolysis, photo-biological water splitting, photo-electrochemical water splitting, and photocatalytic water splitting [26, 27]. However, effectively, and sustainably extracting H_2 from natural sources remains a challenge, and ongoing technological progress is focused on addressing this issue. In 1972, Honda and Fujishima reported the H_2 generation which played a crucial role in the field of H_2 production [26]. Recent years have seen significant progress in photocatalytic H_2 production via water splitting, aiming for near-perfect quantum efficiency [28, 29]. Selecting a photocatalyst involves considering factors such as its light-harvesting efficiency, charge carrier separation capability, stability in water, compatibility with the reaction system, and cost [30, 31].

Graphitic carbon nitride (g-C_3N_4), a material akin to graphene, has recently piqued significant interest in the scientific community due to its exceptional properties in electrocatalysis, photocatalysis, ionic conductivity, electronics, and chemistry [29, 32–34]. The affordability, stability, accessibility, and lightweight nature of g-C_3N_4 have led to its exploration in various applications such as bio-imaging, sensing, water splitting, photocatalysis, and solar cells [35, 36]. Furthermore, the polymer-like structure of g-C_3N_4 indicates its potential for exceptional electrocatalytic properties, leading to its widespread use as a catalyst in detecting harmful substances, toxic metal ions, and biomolecules [37, 38]. Despite being utilized in various fields including optoelectronics, g-C_3N_4 encounters challenges in practical applications due to its low surface area, poor conductivity, and stacked π–π conjugated structure [39]. It is assumed that doping may improve the properties of the g-C_3N_4. Li and his research group [40] studied the photocatalytic activities of C-doped carbon nitride, which exhibited good H_2 production performance. Jiang et al. [41] reported on the incorporation of N, P, and O co-doped carbon into carbon nitride microtubes for H_2 production. Yue et al. [42] achieved an H_2 production rate of 59.5 μmol h^{-1} using Zn-doped carbon

nitride. Zhang et al. [43] reported the synthesis of Na-doped carbon nitride for H_2 production applications, while Huang et al. [44] reported on O-doped carbon nitride for photocatalytic H_2 production. Chen et al. [45] investigated P-doped carbon nitride for H_2 evolution reactions, achieving a notable H_2 evolution rate of 59.1 μmol.h^{-1}. Zhang and co-workers [46] proposed a structure for S-and O-co-doped g-C_3N_4. The above aforementioned reports suggested that doped g-C_3N_4 increased the photocatalytic H_2 evolution compared to the pristine g-C_3N_4. These studies collectively highlight the significant role of doping strategies in enhancing the photocatalytic activity of g-C_3N_4. The platinum (Pt) is one of the efficient co-catalyst which has the potential to enhance the charge transport and improve the H_2 production. Thus, it will be of great significance to explore the Pt cocatalyst for H_2 evolution reactions.

This work proposed the cobalt (Co)-doped g-C_3N_4 (Co@g-C_3N_4) as a photocatalyst for efficient H_2 production of visible light. The Pt was also used as cocatalyst to enhance charge transport and H_2 production. The Co@g-C_3N_4/Pt photocatalyst demonstrated excellent performance for H_2 production with decent reusability.

Materials and methods

Materials and reagents

Cobalt nitrate hexahydrate (ACS reagent, ≥ 98%), urea (ACS reagent, 99%), triethanolamine (TEOA; ≥ 99.0%), sodium sulfide (Na_2S), hexachloroplatinic acid (H_2PtCl_6), and sodium sulfite ($NaSO_3$; ACS reagent, ≥ 98.0%) were purchased from Merck. Methanol (99%), ethanol (94–96%), were bought from Alfa-Aesar. Lactic acid was purchased from Sigma. All the used chemical, reagents and solvents were used as received without any further treatment.

Synthesis of photocatalyst

The Co@g-C_3N_4 photocatalyst was synthesized using calcination of urea in presence of cobalt precursor. In a standard procedure, 6 g of urea and 500 mg of cobalt nitrate hexahydrate were mixed in 10 mL of ethanol with continuous stirring. Further, ethanol was evaporated and residual powder was then transferred to a crucible. This crucible was covered and transferred to the muffle furnace and heated again at 550 ℃ for 2 h [36, 38, 47]. The furnace was allowed to cool down to room temperature (RT) naturally. Finally, the synthesized power was grounded in a mortal pestle. The obtained product was denoted as a Co@g-C_3N_4 photocatalyst. For comparison purposes, pristine g-C_3N_4 was also synthesized using a similar method without the addition of Co precursor.

Instruments

The Hitachi, model S-4800 scanning electron microscope (SEM) has been employed to capture SEM images of the prepared Co@g-C_3N_4 photocatalyst. Horiba EDX instruments were used to obtain the EDS spectrum of the samples. Phase purity and crystallinity of the prepared g-C_3N_4 and Co@g-C_3N_4 photocatalysts were studied using a Rigaku RINT; 2500 V X-ray diffractometer (powder X-ray diffractometer = PXRD). Thermo-scientific X-ray photoelectron spectroscopy (XPS) was utilized to obtain the XPS spectrum of the prepared Co@g-C_3N_4 photocatalyst. The ultraviolet–visible (UV–Vis) spectrum was determined using an Agilent Cary 60 UV–Vis spectrophotometer. The H_2 production studies were conducted using a TCD gas chromatograph.

Photo-catalytic studies for H_2 generation

Photocatalytic H_2 production studies were conducted in a quartz tube reactor, which was sealed to prevent air leakage. Initially, 7 V% methanol (7 mL) was added to 93 mL of water. Subsequently, 50 mg of Co@g-C_3N_4 was added to the solution, followed by the addition of 3 wt% Pt (H_2PtCl_6) as a co-catalyst to improve the photocatalytic activity of the prepared photocatalyst. Nitrogen (N_2) gas was purged through the solution for 60 min to remove dissolved gases. A 150 W LED was used as a visible light source with an intensity of 7.6 mW/cm^2. The evolved H_2 was collected at various time intervals using a syringe and its quantity was determined using gas chromatography. Additionally, different solvents such as ethanol, lactic acid, TEOA, and Na_2SO_3/Na_2S were tested as alternatives to methanol under identical conditions to investigate their effects on the reaction.

Results and discussion

Characterizations

Scanning electron microscopy (SEM) is a powerful technique to characterize the surface morphology of various materials, providing high-resolution images that reveal details at the nanoscale. Thus, we have adopted the SEM technique for the

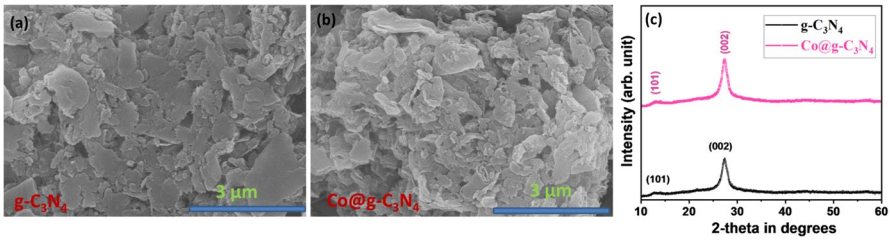

Fig. 1 SEM images of g-C_3N_4 (**a**), and Co@g-C_3N_4 (**b**). XRD spectrum (**c**) of g-C_3N_4 and Co@g-C_3N_4

characterization of surface morphology of the g-C_3N_4 and Co@g-C_3N_4 materials. The flake-like surface structures observed in g-C_3N_4 samples are a result of the unique arrangement of carbon and nitrogen atoms in the synthesized material, as shown in Fig. 1a. Similarly, the SEM image of the Co@g-C_3N_4 materials has been recorded and has been presented in Fig. 1b. The SEM observations also suggested that Co@g-C_3N_4 material has flake-like surface structures which is the characteristic surface morphological feature of g-C_3N_4.

The phase formation, purity, and crystalline nature of the g-C_3N_4 and Co@g-C_3N_4 materials have been studied using the X-ray diffraction (XRD) technique. XRD is a powerful technique used to analyze the crystal structure of materials. The XRD technique may provide valuable insight regarding the formation of the materials along with the crystalline/amorphous nature and phase purity. Hence, XRD patterns of g-C_3N_4 and Co@g-C_3N_4 materials have been obtained at the 2θ range of 10–60º. Fig. 1c presents the XRD results of the prepared g-C_3N_4 and Co@g-C_3N_4 materials. In the case of pure g-C_3N_4 material, two major diffraction peaks have appeared at around 13.5º and 28.78º which can be attributed to the presence of (101) and (002), diffraction planes, respectively. In the case of Co@g-C_3N_4 material, similar peaks have been observed which corresponded to the (101) and (002), diffraction planes of g-C_3N_4. No additional peak has appeared related to Co-based oxide, and it suggested the successful formation of Co@g-C_3N_4 material, as shown in Fig. 1c. The energy dispersive X-ray spectroscopic (EDS) spectrum of the g-C_3N_4 and Co@g-C_3N_4 materials have been recorded to check the elemental composition and phase purity. Fig. S1 shows the EDS spectrum of the g-C_3N_4 and Co@g-C_3N_4 materials. The g-C_3N_4 and Co@g-C_3N_4 materials exhibited the presence of C, N, and C, N, Co elements which confirmed the preparation of g-C_3N_4 and Co@g-C_3N_4 materials.

Photoelectron spectroscopy (XPS) was also applied to further authenticate the successful formation of Co@g-C_3N_4. The high-resolution XPS scans of the Co@g-C_3N_4 are provided in Fig. S2. Fig. S2a shows the C1s spectrum with the presence of sp^2C, C–OH, and C–C bonds. The C–NH, N–$(C)_3$, and N–C = N bonds have been observed in the N 1 s XPS scan, as shown in Fig. S2b. These bonds were related to the g-C_3N_4. The Co2p XPS spectrum has been presented in Fig. S2c which revealed the presence of $Co2p_{1/2}$ and $Co2p_{3/2}$ bonds. The overall results indicated the formation of Co@g-C_3N_4.

Ultraviolet–Visible (UV–Vis) spectroscopy has the potential to provide insights into the optical properties of the obtained g-C_3N_4 and Co@g-C_3N_4. Generally, g-C_3N_4 exhibits absorption in the UV region due to the π–π* transitions of the aromatic system in g-C_3N_4. Fig. 2a shows the UV–Vis data of the obtained g-C_3N_4 and Co@g-C_3N_4. It can be seen that g-C_3N_4 has a broad absorption band around 350–400 nm. The UV–Vis spectrum of the Co@g-C_3N_4 exhibited a similar absorption band with slight shifting towards the visible range. This may be due to the doping of Co to the g-C_3N_4 in the synthesized Co@g-C_3N_4. The band gap of the g-C_3N_4 and Co@g-C_3N_4 was calculated by employing the well-known Tauc relation. Tauc plots are generally used to observe the band gap of synthesized materials from their UV–Vis absorption spectra. The Tauc relation has been described in equation (1) which is given below,

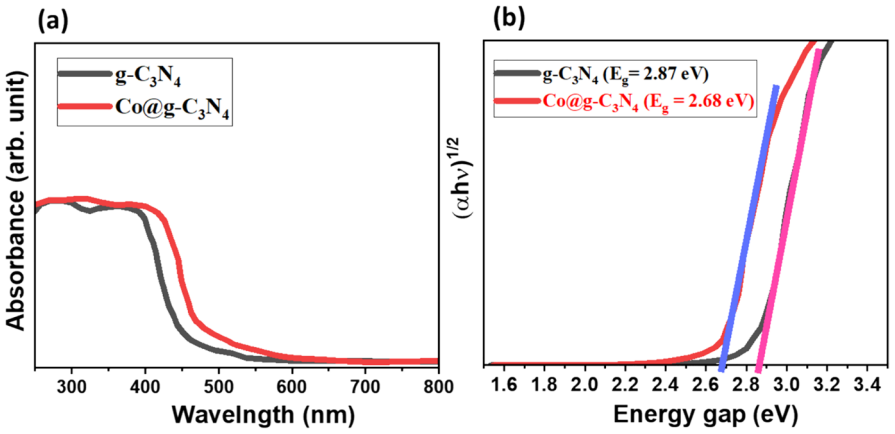

Fig. 2 **a** UV–Vis spectra and **b** Tauc plot of g-C_3N_4 and Co@g-C_3N_4

$$\alpha h\nu = A(h\nu - Eg)^{1/2} \tag{1}$$

(In equation (1), α = absorption coefficient, h = Planck's constant, and ν is the frequency of the incident light, Eg = band gap).

The obtained Tauc plots of the g-C_3N_4 and Co@g-C_3N_4 have been presented in Fig. 2b. It can be seen that g-C_3N_4 and Co@g-C_3N_4 have a band gap of 2.87 and 2.68 eV, respectively. This optical band gap makes them suitable candidate as photocatalysts for their potential applications in photocatalytic H_2 generation.

Hydrogen evolution performance

The H2 production activities of the g-C_3N_4 have been studied using methanol as a scavenger agent. The dose of the g-C_3N_4 was 10 mg and the time of the reaction was 6 h. The produced H_2 has been collected at different times (1–6 h) using a syringe. The obtained H_2 amount has been summarized in Fig. 3a. The H_2 amount of 285 µmol/g has been produced at 6 h for g-C_3N_4-based system. Further, Co@g-C_3N_4 was used under similar conditions and dose of the catalyst.

The obtained results for H_2 production using Co@g-C_3N_4 have been presented in Fig. 3a. The improved H_2 amount of 398 µmol/g has been obtained which showed that Co doping has significantly improved the catalytic properties of the Co@g-C_3N_4. It is well-known that co-catalysts may improve the catalytic properties. Thus, we have used platinum (Pt) as a co-catalyst, and H_2 production activities of the Co@g-C_3N_4/Pt (3 wt%) have been studied under the above-mentioned conditions. The H_2 production amount of Co@g-C_3N_4/Pt (3 wt%) based system has been summarized in Fig. 3a. It can be noted that a further significant change in the H_2 production amount has been observed. The highest H_2 production amount of 450 µmol/g has been obtained after 6 h (Fig. 3b). The Pt further improved the

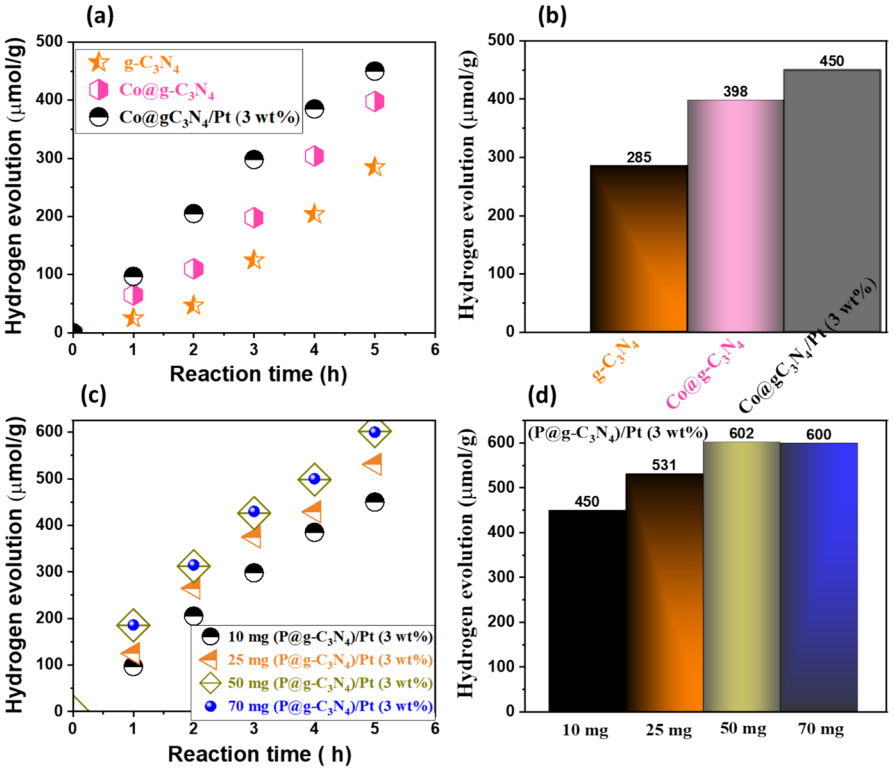

Fig. 3 **a, b** H_2 production amount activities of g-C_3N_4, Co@g-C_3N_4, and Co@g-C_3N_4/Pt (3 wt%) (Catalyst dose = 10 mg) in methanol system at different times. **c, d** H_2 production amount activities of Co@g-C_3N_4/Pt (3 wt%) (Catalyst dose = 10, 25, 50, and 70 mg) in the methanol system at different times

photocatalytic activities and an interesting amount of H_2 production has been achieved using Co@g-C_3N_4/Pt (3 wt%).

The photocatalyst dose may have significant effects on the photocatalytic H_2 production. Thus, it is required to study the effects of different doses of the photocatalyst for H_2 production under similar photocatalytic measurements. In this context, we have used different doses (10, 25, 50, and 70 mg) of the Co@g-C_3N_4/Pt (3 wt%). The obtained results for H_2 generation amounts have been summarized in Fig. 3c, d. It is evident from Fig. 3c, d that the photocatalyst's performance improves with doses up to 50 mg. However, further increases in the photocatalyst dose result in decreased activity. The highest activity, observed at a dose of 50 mg (602 µmol/g), suggests that this amount of photocatalyst is optimal for achieving maximum activity.

It is well-known and reported that different scavengers have different properties and H_2 production can be significantly affected by the presence of scavengers and their properties. In this connection, we have used 50 mg Co@g-C_3N_4/Pt (3 wt%) as photocatalyst and methanol has been replaced with different scavenger agents

(ethanol, triethanolamine = TEOA, lactic acid, and $NaSO_3/Na_2S$). However, other conditions were ideal and the same. Firstly, we studied the H_2 production amount for 50 mg Co@g-C_3N_4/Pt (3 wt%) photocatalyst in the presence of ethanol. The obtained results showed the generation of 726 µmol/g of H_2 amount in the presence of ethanol system, as shown in Fig. 4a. The 50 mg Co@g-C_3N_4/Pt (3 wt%) photocatalyst exhibited an improved H_2 production amount of 3314 µmol/g in the presence of lactic acid. The 50 mg Co@g-C_3N_4/Pt (3 wt%) photocatalyst also demonstrated further improved H_2 production in the presence of Na_2SO_3/Na_2S system. However, the highest H_2 production of 6347 µmol/g has been achieved in the presence of an ethanolamine system. Similarly, the highest H_2 production rate of 1269.4 µmol/g/h has been obtained for 50 mg Co@g-C_3N_4/Pt (3 wt%) photocatalyst in the TEOA system, as shown in Fig. 4b.

Reusability is the most desirable tool for photocatalytic H_2 production, and it is of great significance to study the reusability study for H_2 generation using 50 mg Co@g-C_3N_4/Pt (3 wt%). In this regard, H_2 production activities of the 50 mg Co@g-C_3N_4/Pt (3 wt%) have been studied up to four cycles and observations have been compiled in Fig. 4c. Before every new cycle, the photocatalyst was collected by centrifugation and dried in a vacuum oven and further used for another cycle. The obtained results showed good reusability study up to four cycles. The probable mechanism for the H_2 generation has been described in Fig. S3. It can be assumed that electron–hole pairs are generated on the exposure of Co@g-C_3N_4/Pt to the visible light on the absorption of the photons. The photo-generated electrons in the conduction band of Co@g-C_3N_4 migrated to the surface whereas holes remain in the valence band level. The Pt acted as a co-catalyst and improved electron transportation. The TEOA acted as a sacrificial agent and electron donor. The electrons may be transferred to the surface of Co@g-C_3N_4 and reduce protons (H^+) to form the H_2. The remaining holes in the Co@g-C_3N_4 can oxidize TEOA to form the radicals which can then react with water to generate more electrons and protons. The overall results showed that 50 mg Co@g-C_3N_4/Pt (3 wt%) is the most suitable and optimized photocatalyst for the generation of improved photocatalytic H_2. The H_2 production amount of the 50 mg Co@g-C_3N_4/Pt (3 wt%) has been compared with the previous studies, which are given in Table 1 which is comparable with the reported studies.

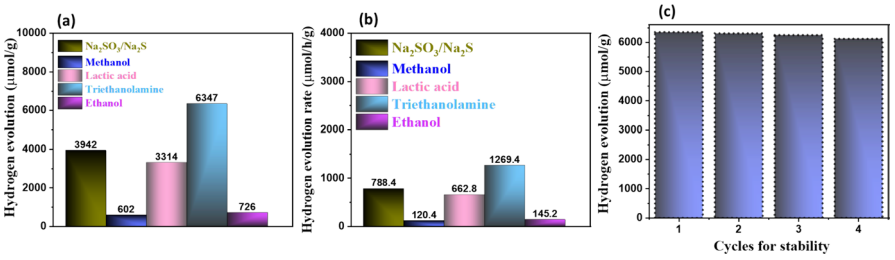

Fig. 4 H_2 production amount (**a**) and H_2 production rate (**b**) of 50 mg Co@g-C_3N_4/Pt (3 wt%) photocatalyst in the presence of different scavenger agents (methanol, ethanol, TEOA, lactic acid, and $NaSO_3/Na_2S$). (**c**) Reusability study for 50 mg Co@g-C_3N_4/Pt (3 wt%) photocatalyst in TEOA system

Table 1 Comparison of the H_2 production of 50 mg Co@g-C_3N_4/Pt (3 wt%) with previous studies [43–49]

Photocatalyst	H_2 evolution (μmol/g.h)	Photocatalysts weight (mg)	Light source	References
g-C_3N_4	449.86	50	300 W Xe-lamp	[48]
MoS_2@g-C_3N_4	1020	10	450 W Xe-lamp	[49]
$NiFe_2O_4$@Cu_2O	3.98	100	250 W metal halides lamp	[50]
O@g-C_3N_4	1045	50	300 W Xe lamp	[51]
CoS_2@MoS_2-g-C_3N_4	375	20	300 W Xe lamp	[52]
S@g-C_3N_4-$BiVO_4$	750	20	300 W Hg (Xe) DC Arc lamp	[53]
g-C_3N_4/WO_3	110	40	300 W Xe lamp	[54]
Co@g-C_3N_4/Pt (3 wt%)	1270	50	150 W LED	Present work

Conclusions

In this conclusion section, it is worthy to state that Co@g-C_3N_4 has been obtained using urea as a precursor. Furthermore, photocatalytic hydrogen production activities of the Co@g-C_3N_4 have been checked in the presence of a methanol scavenger agent. The Pt has been introduced as a cocatalyst and Co@g-C_3N_4/Pt (3wt%) exhibited good performance. The dose of the Co@g-C_3N_4/Pt (3wt%) has been optimized and 50 mg Co@g-C_3N_4/Pt (3wt%) showed the highest performance. Furthermore, different solvents have been applied and Co@g-C_3N_4/Pt (3wt%) demonstrated excellent photocatalytic H_2 generation activity of more than 6000 μmol/g in the presence of TEOA scavenger agent. The Co@g-C_3N_4/Pt (3wt%) also demonstrated good reusability studies.

Supplementary Information The online version contains supplementary material available at https://doi.org/10.1007/s11144-024-02663-5.

Acknowledgements Authors gratefully acknowledged Researchers Supporting Project Number (RSP2024R78), King Saud University, Riyadh, Saudi Arabia.

Data availability Data will be availbale on reasonable request.

Declarations

Conflicts of interests Authors declare no conflicts of interest.

References

1. Ahmad K, Ansari SN, Natarajan K, Mobin SM (2019) ChemElectroChem 6:1192–1198
2. Zhang X, Matras-Postolek K, Yang P, Ping Jiang S (2023) J Colloid Interface Sci 636:646–656
3. Ahmad K, Song G, Kim H (2022) ACS Sustain Chem Eng 10:11948–11957
4. Ahmad K, Kim H (2022) Mater Lett 318:132187

5. Zhang X, Yang P (2023) ChemNanoMat 9:e202300041
6. Kumar P, Ahmad K, Dagar J et al (2021) ChemElectroChem 8:3150–3154
7. Ahmad K, Shinde MA, Song G, Kim H (2021) Ceram Int 47:34297–34306
8. Ahmad K, Khan MQ, Khan RA, Kim H (2022) Opt Mater 128:112458
9. Ye S, Wang R, Wu MZ, Yuan YP (2015) Appl Surf Sci 35:15–27
10. Gong D, Highfield JG, Ng SZE et al (2014) ACS Sustain Chem Eng 2:149–157
11. Mittal G, Dhand V, Rhee KY, Park SJ, Lee WR (2015) J Indus Eng Chem 21:11–25
12. Osuagwu B, Raza W, Tesler AB, Schmuki P (2021) Nanoscale 13:12750–12756
13. Raza W, Ahmad K, Khan RA, Kim H (2023) Int J Hydrog Energy 48:29071–29081
14. Liu J, Cheng B, Yu J (2016) Phys Chem Chem Phys 18:31175–31183
15. Ahmad K, Kumar P, Kim H, Mobin SM (2022) ChemNanoMat 8:e202200061
16. Raza W, Ahmad K (2021) Artificial photosynthesis system for the reduction of carbon dioxide to value-added fuels. Handbook of greener synthesis of nanomaterials and compounds: volume 1: Fundamental principles and methods. Elsevier, Amsterdam, pp 917–938
17. Miao Z, Wu G, Wang Q, Yang J, Wang Z, Yan P, Sun P, Lei Y, Mo Z, Xu H (2023) Mater Rep Energy 3:100235
18. Ahmad K, Khan MQ, Kim H (2022) Opt Mater 128:112374
19. Ahmad K, Shinde MA, Kim H (2021) Microchem J 169:106583
20. Ahmad K, Raza W, Khan MQ (2021) Water splitting: Design, synthesis and fabrication of nanostructured materials based efficient electrodes for water splitting applications. Handbook of greener synthesis of nanomaterials and compounds: volume 2: Synthesis at the macroscale and nanoscale. Elsevier, Amsterdam, pp 549–564
21. Gorai DK, Kundu T (2020) Influence of Pt and P doping on the performance of g-C_3N_4 monolayer. Mater Manufac Processes 35:625–634
22. Navidpour AH, Hao D, Li X, Li D, Huang Z, Zhou L (2023) Catal Rev 1:72
23. Yue B, Li Q, Iwai H, Kako T, Ye J (2011) Sci Technol Adv Mater 12:3
24. Zhong Z, Fang J, Hu K et al (2023) CSEE J Power Energy Syst 9:1266–1283
25. He R, Liang H, Li C, Bai J (2020) A Physicochem Eng Asp 586:124200
26. Fujishima A, Honda K (1972) Nature 238:37–38
27. Wang N, Li J, Wu L et al (2016) Int J Hydrog Energy 41:22743–22750
28. Mun SJ, Park SJ (2019) Catalysts 9:805
29. Ahmad K, Chaudhary A, Raza W et al (2023) Opt Mater 140:113857
30. Takata T, Jiang J, Sakata Y et al (2020) Nature 581:411–414
31. Wang Z, Li C, Domen K (2019) Chem Soc Rev 48:2109–2125
32. Raza W, Ahmad K (2022) Graphitic carbon nitride-based photocatalysts for hydrogen production. Sustainable materials and green processing for energy conversion. Elsevier, Amsterdam, pp 213–236
33. Ahmad K, Raza W, Alsulmi A, Kim H (2023) Diam Relat Mater 138:110178
34. Zhu J, Xiao P, Li H, Carabineiro SAC (2014) ACS Appl Mater Interfaces 6:16449–16465
35. Patnaik S, Martha S, Parida KM (2016) RSC Adv 6:46929–46951
36. Raza W, Bahnemann D, Muneer M (2017) J Photochem Photobiol A Chem 342:102–115
37. Cao S, Low J, Yu J, Jaroniec M (2015) Adv Mater 27:2150–2176
38. Sewnet A, Alemayehu E, Abebe M, Mani D, Thomas S, Kalarikkal N, Lennartz B (2023) Nanomater 13:762
39. Amiri M, Salehniya H, Habibi-Yangjeh A (2016) Ind Eng Chem Res 55:8114–8122
40. Wang H, Huang G, Chen Z, Li W (2018) Catalysts 8:366
41. Jiang L, Guo Y, Pan J et al (2022) Sci Total Environ 809:151114
42. Yue B, Li Q, Iwai H et al (2011) Sci Technol Adv Mater 12:34401–34408
43. Zhang L, Ding N, Hashimoto M et al (2018) Nano Res 11:2295–2309
44. Huang J, Wang H, Yu H et al (2020) Chemsuschem 13:5041–5049
45. Chen L, Yan G, Liu X et al (2022) Phys Chem Chem Phys 25:117–123
46. You R, Dou H, Chen L et al (2017) RSC Adv 7:15842–15850
47. She P, Yao C, Li J et al (2021) Mater Res Express 8:125006
48. Liu M, Jiao Y, Qin J et al (2021) Appl Surf Sci 541:148558
49. Wang M, Ju P, Zhao Y et al (2018) New J Chem 42:910–917
50. Domínguez-Arvizu JL, Jiménez-Miramontes JA, Hernández-Majalca BC et al (2022) J Mater Res Technol 21:4184–4199
51. Yang L, Huang J, Shi L et al (2017) Appl Catal B Environ 204:335–345

52. Liang H, Zhang Q, Bai J et al (2023) Diam Relat Mater 134:109764
53. Kong HJ, Won DH, Kim J, Woo SI (2016) Chem Mater 28:1318–1324
54. Katsumata H, Tachi Y, Suzuki T, Kaneco S (2014) RSC Adv 4:21405–21409